energies

MDPI

Article

Implementation Strategy of Test Facility Based on Auto-Transformer for LVRT/HVRT Evaluation of Large-Scale Wind Turbine

Byungki Kim *, Yang-Hyun Nam, Kyung-Sang Ryu and Dae-Jin Kim *

Jeju Global Research Center (JGRC), Korea Institute of Energy Research (KIER), 200 Haemajihaean-ro, Gujwa-eup, Jeju 63357, Jeju Specific Self-Governing Province, Republic of Korea
* Correspondence: bk_kim@kier.re.kr (B.K.); djk@kier.re.kr (D.-J.K.); Tel.: +82-64-800-2218 (B.K.)

Abstract: In accordance with South Korea's recent 2030 Carbon Neutral Plan, an 8GW offshore wind farm is planned for construction in the South-west Sea. Therefore, it is expected that large-scale wind turbines will be installed, and these turbines must operate stably, even when there are instantaneous voltage fluctuations in the power system. The grid code is described for the low-voltage-ride-through (LVRT) and high-voltage-ride-through (HVRT) functions, and a test facility that can perform both LVRT and HVRT tests is essential. In the case of LVRT/HVRT test facilities developed by the existing RLC (impedance component) method, it may be difficult to test large-scale wind turbines due to problems such as power quality, frequent failures and narrow short-circuit capacity ranges. Therefore, to solve such problems, this paper proposes an LVRT/HVRT test facility of the autotransformer type, which is capable of outputting the desired voltage range by changing the wiring method and tap position. Specifically, in order to implement the test facility of the autotransformer type, which is able to output the desired voltage range by changing the wiring method and tap according to the LVRT/HVRT test status, this paper presents an impedance determination algorithm (two-step layer impedance determination algorithm) of auto-transformer based on the fault-current analysis and operation strategy at a real LVRT/HVRT testing evaluation facility.

Keywords: low voltage ride through; high voltage ride through; wind turbine auto-transformer; implementation strategy

check for updates

Citation: Kim, B.; Nam, Y.-H.; Ryu, K.-S.; Kim, D.-J. Implementation Strategy of Test Facility Based on Auto-Transformer for LVRT/HVRT Evaluation of Large-Scale Wind Turbine. *Energies* **2023**, *16*, 4194. https://doi.org/10.3390/en16104194

Academic Editors: Davide Astolfi and Abu-Siada Ahmed

Received: 7 March 2023
Revised: 28 April 2023
Accepted: 16 May 2023
Published: 19 May 2023

Copyright: © 2023 by the authors. Licensee MDPI, Basel, Switzerland. This article is an open access article distributed under the terms and conditions of the Creative Commons Attribution (CC BY) license (https://creativecommons.org/licenses/by/4.0/).

1. Introduction

Recently, Korea has planned to build a wind farm of 8 GW or more and a large-capacity wind farm complex off-shore of the Southwest Sea region according to the global trend, which is being jointly promoted for de-carbonization. Under these concepts, large wind turbines (WT) must be maintained in a stable manner during the moments of voltage drops or rises caused by instantaneous faults in the power system. In particular, large-scale wind turbines are rotating machines with inertia problems which are, a lot of the time, required to be re-started when disconnected by abnormal states in the grid. Therefore, there is the possibility that outages could occur due to large fluctuations in frequency when large-scale wind turbines are disconnected from the grid by temporary voltage fluctuations and a similar case was reported in Australia in 2019 [1]. On the other hand, in order to prevent the wind turbine from dropping out by the instantaneous voltage rise or drop in the grid, IEC 61400-21-1 is presenting a test procedure and evaluation method for LVRT/HVRT that can evaluate the dynamic performance of wind turbine, as shown in Figure 1 [2,3]. In addition, a functional test of LVRT/HVRT for new and renewable energy sources, including large-scale wind turbines, is also recommended by the domestic transmission and distribution system usage regulation (grid code in South Korea), revised in 2020 [4].

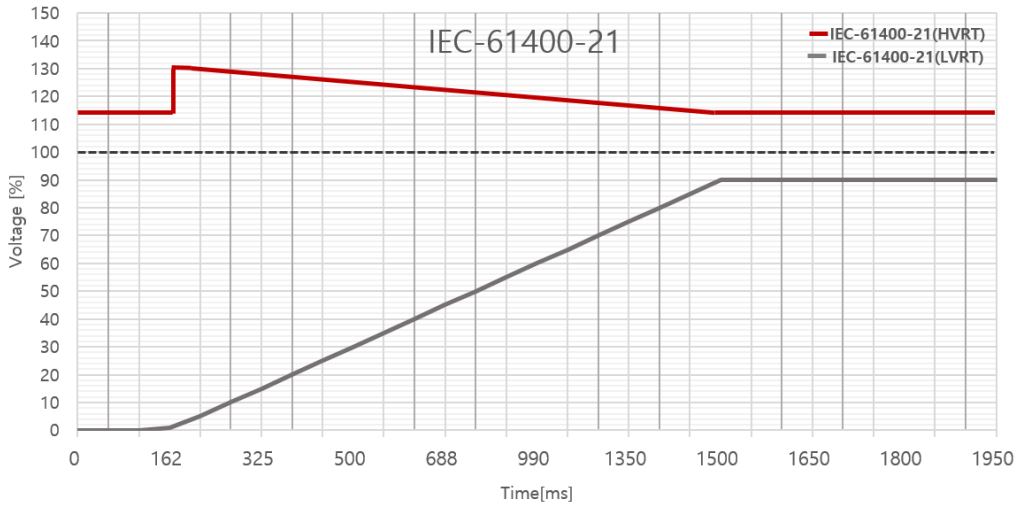

Figure 1. LVRT/HVRT Standard Curve of IEC 61400-21-1.

On the other hand, refs. [5–10] is only presented to LVRT control schemes for the wind turbines of the PMSG and DFIG types. Furthermore, refs. [11–13] proposes an LVRT test method of ESS (grid forming converter) using a grid simulator. As the operation of these LVRT/HVRT functions is required by the grid code, it is necessary to develop a facility that can perform both LVRT and HVRT tests for large-scale wind turbines. In the case of the implementation of HVRT characteristics using the test facility with the existing RLC method, it is difficult to carry out the testing of large-scale wind turbines due to problems such as power quality, frequent failures and narrow short-circuit capacity range etc. [12,13]. Furthermore, a test facility for the LVRT test as an alternative to the impedance-based approach has already been presented in previous papers in the literature [14–17]. Therefore, comparison between the previous methods and proposed method is summarized in Table 1.

Table 1. Comparison of previous methods and proposed method.

Ref.	Contents	
	Previous Methods	**Proposed Method**
[5–10]	- Presented to LVRT control scheme for the wind turbine of PMSG and DFIG type.	- Proposed a detailed calculation method of series/parallel impedance by each voltage level using proposed fault characteristics-based LVRT/HVRT impedance determination method and successive approximation method
[12,13]	- (RLC method) Difficulty in carrying out the test for large-scale wind turbines due to problems such as power quality, frequent failures and narrow short-circuit capacity range	- (autotransformer type) suitable for the test for large-scale wind turbines due to the advantage of implementing voltages into the wide range
[14–17]	- Already presented in previous papers, these papers mainly focus on the generation of the voltage waveforms and on the implemented control algorithm for the test equipment	- LVRT/HVRT test facility of autotransformer type in which it is possible to output the desired voltage range by changing the wiring method and tap position - Differential operation strategy considering the LVRT/HVRT wiring method in order to perform a stable test when the wind turbine generates power normally

To overcome such a problem, this paper proposes an LVRT/HVRT test facility of the autotransformer type, which is capable of outputting the desired voltage range by changing the wiring method and tap position. This method has the advantage that the voltage level can be flexibly adjusted by changing the tap. Furthermore, the LVRT/HVRT facility-based autotransformer type is suitable for the test for large-scale wind turbines due to the advantage of implementing voltages in a wide range [18,19]. In order to implement the test facility of autotransformer type, which is capable of outputting the desired voltage by tap changing according to the LVRT/HVRT test status, this paper presents an impedance determination algorithm (two-step layer impedance determination algorithm) of auto-transformer based on the fault-current analysis.

Namely, to obtain the turn ratio and tap position of the series/parallel winding, this paper proposes the two-step layer impedance determination algorithm that combines a calculation method based on fault-current analysis/impedance map and successive approximation method. However, it is possible that the required voltage levels in LVRT/HVRT are not satisfied due to a voltage drop due to series impedance, even though the current, which is determined by parallel impedance, is kept within the allowable range (Based on three times the short circuit ratio). Therefore, the second step presents the successive approximation method, which calculates the optimal value by successively fixing the impedance parameters in order to obtain the series and parallel impedances for the voltage range of LVRT and HVRT.

Furthermore, this paper presents a differential operation strategy considering LVRT/HVRT wiring method in order to perform a stable test when the wind turbine generates power normally. In order to prepare an environment in which the LVRT/HVRT control function of a wind turbine can be verified in advance, LVRT/HVRT tests were performed through the implementation of a 30 kW-scale artificial LVRT/HVRT test facility and a wind turbine hardware-in-loop evaluation system with real-time signal processing technology. A 30 kW-scale artificial LVRT/HVRT test facility was implemented using a two-step layer impedance decision algorithm and differential operation strategies of the test facility.

The main contributions are summarized as follows:

- A 30 kW-scale artificial LVRT/HVRT test facility implemented by impedance determination algorithm and operation strategy is confirmed that can be stably applied for the LVRT/HVRT field test of a large-scale wind turbine;
- From systematical simulation analysis and test by the artificial test simulator, it shows that LVRT/HVRT facility-based autotransformer can efficiently perform as a test facility for large-scale wind turbines and has the advantage of implementing voltages in a wide range;
- Through the proposed impedance determination algorithm, it is confirmed that a test facility can be stably developed for a 12 MW-scale LVRT/HVRT facility.

2. Characteristics of the LVRT/HVRT Test Facility for Wind Turbines

2.1. Characteristics of the LVRT/HVRT Test Facility

As shown in Figure 2, an autotransformer composed of one winding is divided into series winding and parallel winding through an intermediate tap; the input voltage can be raised or dropped depending on the circuit and tap configuration. By considering the circuit configuration for the voltage rise function of the autotransformer, as shown in Figure 2a, this is implemented as the LVRT of the test facility. The HVRT characteristics of the test facility are simulated by using circuit configuration for the voltage drop function of the autotransformer, as expressed in Figure 2b. In addition, the LVRT/HVRT test facility of tap-changer type based on the autotransformer has the advantage of being able to flexibly adjust the voltage level by changing the turns ratio of the series-parallel windings.

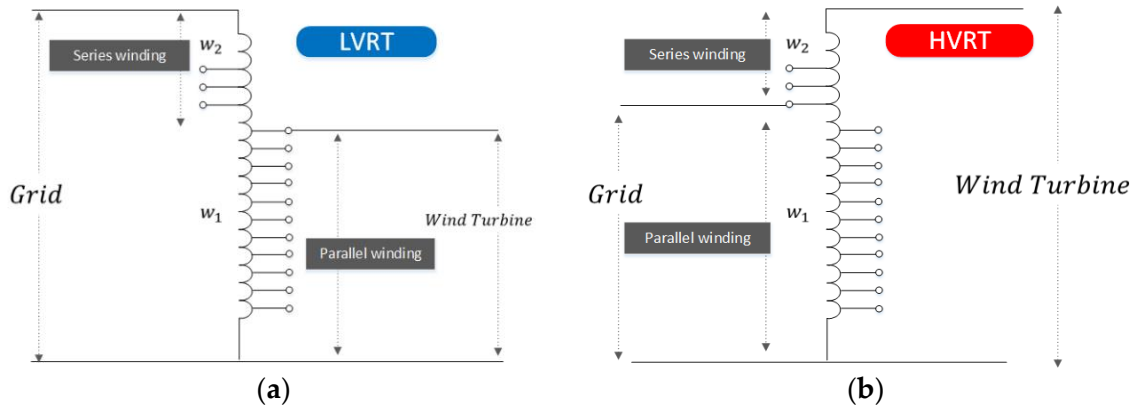

Figure 2. LVRT/HVRT function-based tap changer type. (**a**) LVRT Concept. (**b**) HVRT Concept.

Under these concepts, to develop a 12 MW-scale LVRT/HVRT test facility, this paper adopts the autotransformer type, which can output the desired voltage by changing the tap according to the LVRT/HVRT test status, as shown in Figure 3 and Table 2.

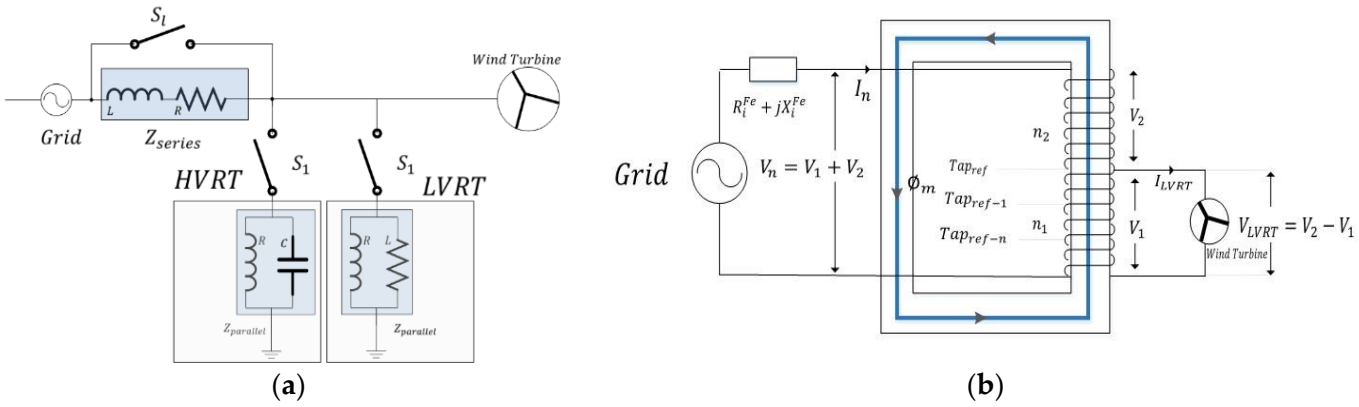

Figure 3. Circuit configuration of RLC and transformer types. (**a**) RLC type. (**b**) Transformer type.

Table 2. Comparison of RLC and transformer types.

Impedance (Existing)	Transformer (Proposed)
- Large installation space	- Narrow installation space
- Narrow short-circuit capacity	- Wide short-circuit capacity
- Requires many RLC elements and frequent maintenance	- Variable by applying an air-core transformer design and a separate impedance core
- High maintenance cost due to damage of capacitance by high current during the test	- Less possibility of maintenance cost due to the allowable capacity of the transformer

2.2. Modeling of LVRT and HVRT Test Facility

The maximum voltage range of HVRT recommended by IEC-61400-21-1 is 130%, and the minimum voltage range of LVRT is 0%. Therefore, For the LVRT/HVRT test facility with a voltage adjustment range between 0–130%, the turns ratio for series/parallel windings and the number of taps is determined by the total desired voltage level (step). As mentioned above, the concept of an LVRT/HVRT test facility using an autotransformer is expressed in Figure 4. Where, V_{Target}^{HVRT} means HVRT range between 100–130% and V_{Target}^{LVRT} means an LVRT range between 0% and 100%.

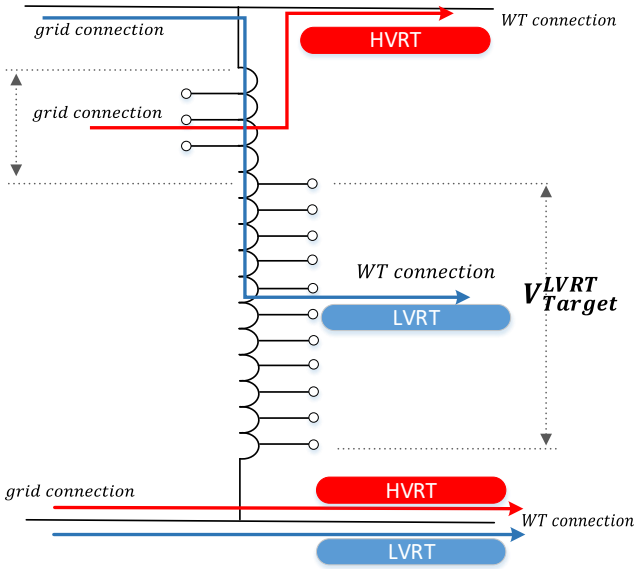

Figure 4. Concept for the tap connection method of LVRT/HVRT.

To implement the LVRT/HVRT test equipment, this paper proposes a method for determining the turn ratio series/parallel windings and tap position according to the desired voltage level. First, the turn ratio of the parallel winding, $W_{1,}$ and the series winding, $W_{2,}$ of LVRT and HVRT is determined by the ratio characteristic of the rated voltage and the desired test voltage, as shown in Equations (1) and (2). From the calculation equations for the turns ratio, the rated voltage is assumed to be a reference value in LVRT expressed by Equation (1), and the desired test voltage is considered as a reference value in HVRT, as shown in Equation (2). In calculating the turn ratio, the sum of the parallel winding, $W_{1,}$ and the series winding, $W_{2,}$ always converges to one.

$$\text{LVRT}(W_{1x} : W_{2x}) = \frac{V_{Target}}{V_n} \times V_n : \frac{V_{Target}}{V_n} \times \left|V_n - V_{Target}\right| \quad (1)$$

$$\text{HVRT}(W_{1x} : W_{2x}) = \frac{V_n}{V_{Target}} \times V_n : \frac{V_n}{V_{Target}} \times \left|V_n - V_{Target}\right| \quad (2)$$

where, W_1 is the turns ratio of parallel windings at x percent unit, W_2 is the turns ratio of series winding at x percent and V_{Target} is the target test voltage.

3. The Two-Step Layer Impedance Determination Algorithm of the LVRT/HVRT Test Facility

In general, the voltage becomes zero, and the current is determined by the grid impedance when a short circuit fault occurs in the grid. In the case of simulating the voltage of 0 PU in the LVRT characteristic test, the impedance of the series winding reaches the maximum and the impedance of the parallel winding approaches zero. In this case, damage or malfunction may occur in test devices and the main circuit breaker on the grid side due to the fault current, which may exceed the allowable limit if the series-parallel impedance of the transformer is determined without considering the capacity of the test devices during the 0 PU voltage simulation. Therefore, this paper proposes a method of calculating the impedance of the series-parallel winding by considering the turn ratio of the transformer at each voltage level based on the calculated impedance of the series winding that can be limited to three times the capacity of the test facility. It is also possible that voltages of each test level cannot be satisfied as the occurrence of voltage drop by series impedance, even if the current determined by the impedance (series-parallel) has a value within the allowable range of the test facility (based on three times to the short-circuit ratio). Therefore, this paper presents a successive approximation method, which calculates the

optimal value by sequentially fixing the impedance parameters in order to obtain the series and parallel impedances for each test voltage value that satisfies the allowable voltage and current in the LVRT and HVRT ranges. Ultimately, this paper proposes a two-step layer impedance determination algorithm which is determined by considering both the fault characteristic-based LVRT/HVRT impedance determination method and successive approximation method.

3.1. Impedance Determination Based on an Impedance Map

The positive phase-sequence % impedance map is designed by the distribution diagram interconnected with a wind turbine, as shown in Figure 5. The distribution diagram includes the impedance for the substation bus, main transformer, cable impedance, and service transformer. Furthermore, the magnitude of transient reactance is minimized as it is assumed that there is no instantaneous influence from the wind power generator.

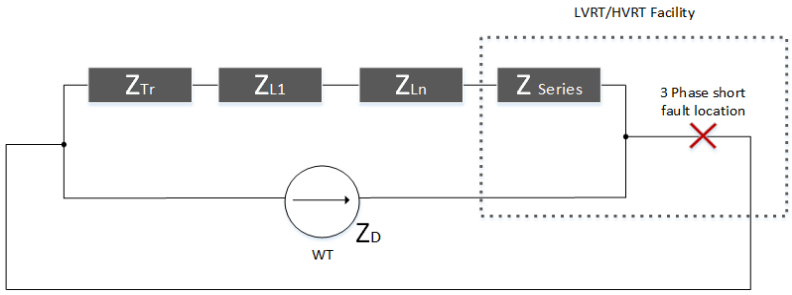

Figure 5. Impedance map.

Under this concept, the total impedance for analysis of the fault current can be calculated by Equation (3) based on the impedance map in Figure 5.

$$\%Z_{total} = (Z_{tr} + Z_{L1} + \sum_{i=1}^{n}(Z_{Li}) + Z_s^{max}) \quad (3)$$

where $\%Z_{total}$ is the total impedance (positive phase sequence), Z_{tr} is the main transformer impedance, Z_{L1} is the bus impedance, Z_{Li} the is i^{th} line impedance, Z_s^{max} is the maximum series impedance for the test facility, Z_D is the wind turbine impedance (including service transformer impedance), i is the section number and n is the number of total sections.

The three-phase short-circuit fault current is calculated based on the above-mentioned impedance map. As shown in Equation (4), the fault current of the LVRT is determined by considering the capacity of the test facility and the short-circuit ratio (a: three times), according to the reference recommendation of IEC-61400-21. As a constraint, the fault current should be determined within three times the rated capacity of the test facility, as shown in Equation (5). Fault current means the sum of the incoming current at the grid side and the incoming current at the wind turbine side.

$$I_{3s}^{tar} = \left(\frac{100}{\%Z_{total}} \times \frac{Base\ kVA_{tr}}{\sqrt{3} \times V_n}\right) + \left(\frac{100}{\%Z_D} \times \frac{Base\ kVA_{WT}}{\sqrt{3} \times V_n}\right) \quad (4)$$

$$Subject\ to \quad I_{3s}^{tar} \leq a \cdot \frac{P_{facility}}{\sqrt{3} \times V_n} \quad (5)$$

where I_{3s}^{tar} is the desired three-phase short-circuit current considering the facility capacity, a is the weight factor of the current magnitude (referenced LVRT: three), $Base\ kVA_{tr}$ is the reference capacity of the main transformer for fault current calculation, $Base\ kVA_{WT}$ is the reference capacity of the wind turbine at the EUT (equipment underside) and V_n is the line-to-line voltage (nominal voltage).

From the three-phase short circuit calculation method in Equation (6) above, the total impedance of the test facility is calculated as shown in Equation (7); here, $\%Z_{max}$ means the maximum value of the series impedance when the voltage level is assumed to be 0 PU.

$$\%Z_s^{max} = \left(\frac{100}{\left(I_{3s}^{tar}\right) - \left(\frac{100}{\%Z_D} \times \frac{Base\ kVA_{WT}}{\sqrt{3} \times V_n}\right)} \times \frac{Base\ kVA_{tr}}{\sqrt{3} \times V_n} \right) - Z_{tr} - \sum_{i=1}^{n}(Z_{L1} + Z_{Li}) \quad (6)$$

$$Subject\ to\ \%Z_s^{max} = \{maximum\%Z_{serise}, V_{lvrt} = 0PU\} \quad (7)$$

where $\%Z_{s.max}$ is the maximum percentage value of series impedance at 0 PU.

To calculate the series-parallel impedance value, $\%Z_{s.max}$ is converted to impedance as follows:

$$L_{capa}^{max}[H] = \frac{\%Z_s^{max} \times V_n^2 \times 10}{2\pi f \times Base\ KVA_{tr}} \quad (8)$$

where $L_{capa}^{max}[H]$ is the maximum impedance (reactance).

Based on the maximum value of the series impedance ($\mathrm{L}_{\mathrm{capa}}^{\mathrm{max}}[\mathrm{H}]$) at 0PU, which is determined in Equation (9), the target series and parallel impedance according to the voltage fluctuation range, as presented in Table 3, are calculated by Equation (9).

$$xPU(L_p : L_s) = L_{max} \times w_{1x} : L_{max} \times w_{2x} \quad (9)$$

$$\forall x = 0, 0.1, \cdots, 1.3[PU]$$

where L_p and L_s are the series and parallel impedance at xPU (Voltage), w_{1x} is parallel impedance ratio in case xPU, w_{2x} is the series impedance ratio in the case of xPU, and x is the voltage percent unit value.

Table 3. Series and parallel impedance ratio according to the state of LVRT and HVRT impedance.

Voltage (*x PU*)	**HVRT**		**Voltage (*x PU*)**	**LVRT**	
	Z_s^{xPU}	Z_p^{xPU}		Z_s^{xPU} **Ratio**	Z_p^{xPU} **Ratio**
	w_{1x}	w_{2x}		w_{1x}	w_{2x}
1.3	0.23	0.77	0.9	0.1	0.9
			0.8	0.2	0.8
1.25	0.2	0.8	0.7	0.3	0.7
			0.6	0.4	0.6
1.2	1.67	0.83	0.5	0.5	0.5
1.15	1.3	0.87	0.4	0.6	0.4
			0.3	0.7	0.3
1.11	0.9	0.91	0.2	0.8	0.2
			0.1	0.9	0.1
1.05	0.5	0.95	0	0.99	0.01

As mentioned above, the impedance determination algorithm based on the impedance map of a one-step layer is shown in Figure 6.

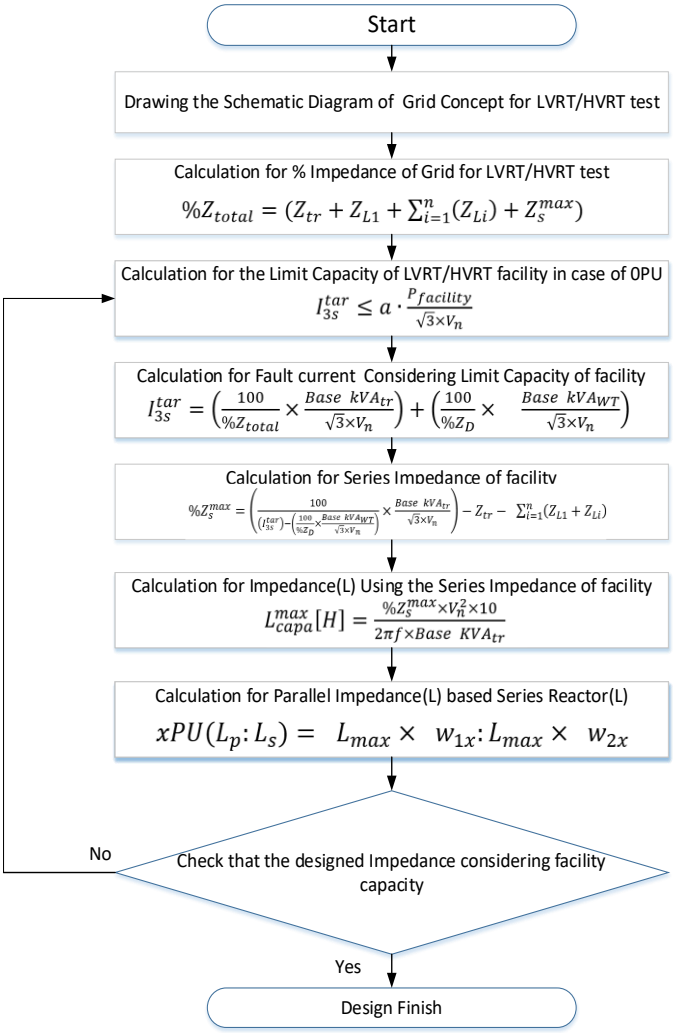

Figure 6. Impedance calculation algorithm based on impedance map.

3.2. Successive Approximation Method Using a Two-Step Layer

The desired voltage levels in the LVRT/HVRT test can be possible that is not satisfied due to a voltage drop by series impedance, even though the current, which is determined by parallel impedance, is kept within the allowable range (Based on three times the short circuit ratio). Therefore, this paper presents a successive approximation method that calculates optimal value by successively fixing the impedance parameters in order to obtain the series and parallel impedances for the voltage range of LVRT and HVRT [16].

First of all, this series/parallel impedance, calculated using the impedance estimation method based on the fault current, is assumed as the initial value.

Then, the voltage drop considering the series impedance (Z_p^{xPU}) and the line impedance is calculated by using Equation (10) by constantly changing the parallel impedance of the LVRT facility based on the initial value.

$$\Delta V = V_{grid} - (\sum_{i=1}^{n} Z_{Li} + Z_{L1} + Z_s^{xPU}) \times (\frac{V_n}{Z_p^{xPU}}) \times COS\theta \quad (10)$$

where V_{grid} is the grid voltage and Z_s^{xPU} is series impedance of target voltage dip.

Meanwhile, if the magnitude of the voltage dip calculated from Equations (11) and (12) is smaller than the ones of all voltage levels, it is considered that the adjusted series-parallel impedance is applicable.

$$V_{dip}(k,z) < \Delta V \; \forall \; K = 0.01 \cdots 1.3PU \tag{11}$$

$$Z = \begin{cases} LVRT \; if \; K = 0.01 \cdots 0.9 \\ HVRT \; if \; K = 1.05 \cdots 1.3 \end{cases} \tag{12}$$

where $V_{dip}(k,z)$ is the target voltage for LVRT and HVRT, K is the facility voltage dip and Z is the voltage dip based on the condition for LVRT and HVRT.

Even though the voltage conditions are satisfied, the series impedance is re-adjusted using Equation (9) in order to match the parallel impedance if the proportion of the turn ratio between the series and parallel impedance is not identical. In order words, the series/parallel impedance that which are satisfied for voltage level is re-calculated by repeating the above-mentioned process from Equation (9) to Equation (12). In order words, in order to obtain the series and parallel impedances for the voltage range of LVRT and HVRT, calculating the optimal value is repeatedly carried out by successively fixing the impedance parameters, as mentioned earlier. The flowchart for the successive approximation method is shown in Figure 7.

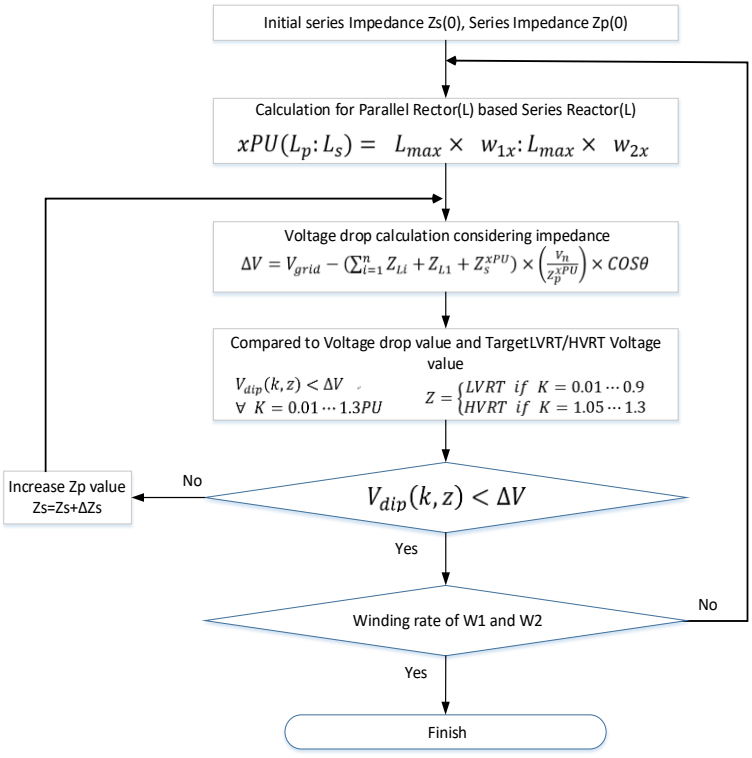

Figure 7. Impedance determination algorithm using a successive approximation method.

Therefore, this paper proposes a detailed calculation method of series/parallel impedance by each voltage level using the proposed fault characteristics-based LVRT/HVRT impedance determination and successive approximation methods, as shown in Figure 8. Furthermore, the procedure for the two-step layer impedance determination algorithm by considering both of these methods can be expressed as follows.

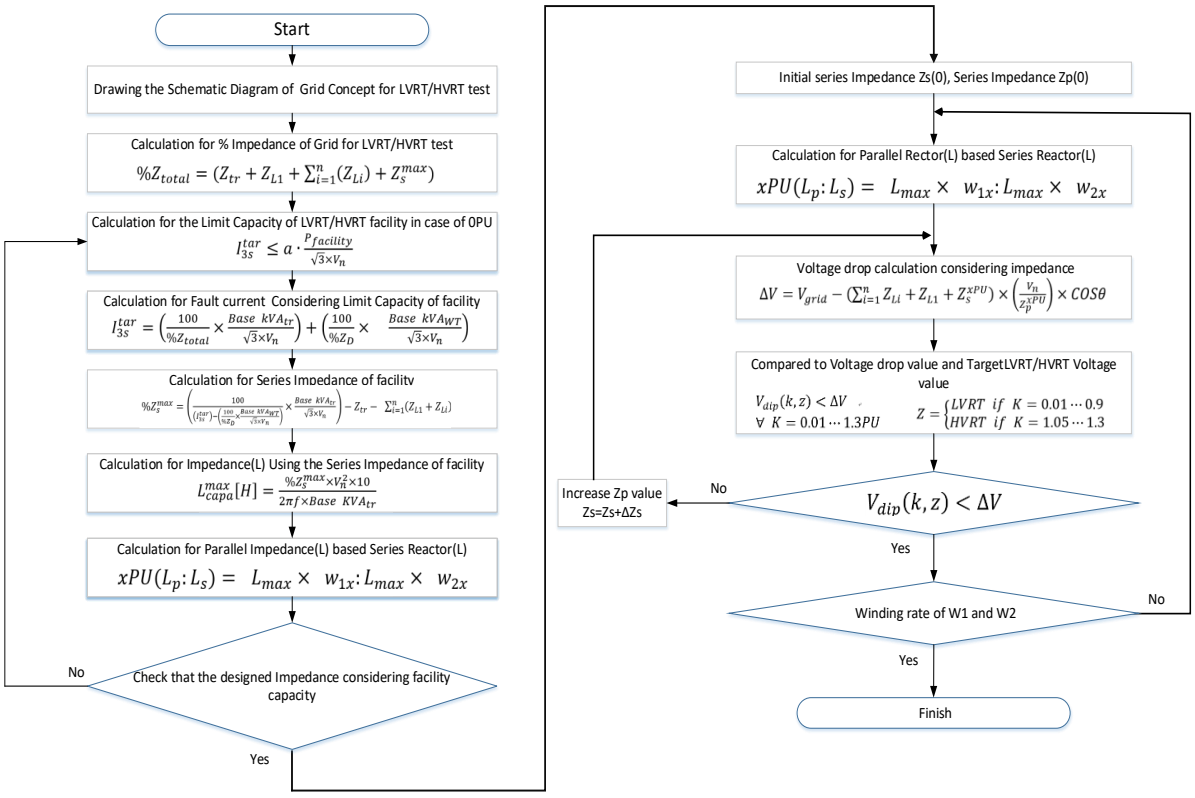

Figure 8. Two-step layer impedance determination algorithm.

4. Differential Operation Procedure of the LVRT/HVRT Test Facility-Based Autotransformer

For the operation of an LVRT/HVRT test facility, the wiring method of the autotransformer should be changed according to the overvoltage (HVRT) test and undervoltage (LVRT) tests. Under these concepts, this paper proposes a differential operation strategy considering LVRT/HVRT wiring method to perform the stable test when the wind turbine generates power normally. As shown in Figure 9, the test facility is composed of a bypass (Bypass-MC1) circuit breaker that is directly connected to the grid and the wind turbine, a selection circuit breaker and a control circuit breaker. Where, LVRT/HVRT characteristic test is performed only when the wind turbine generates power normally.

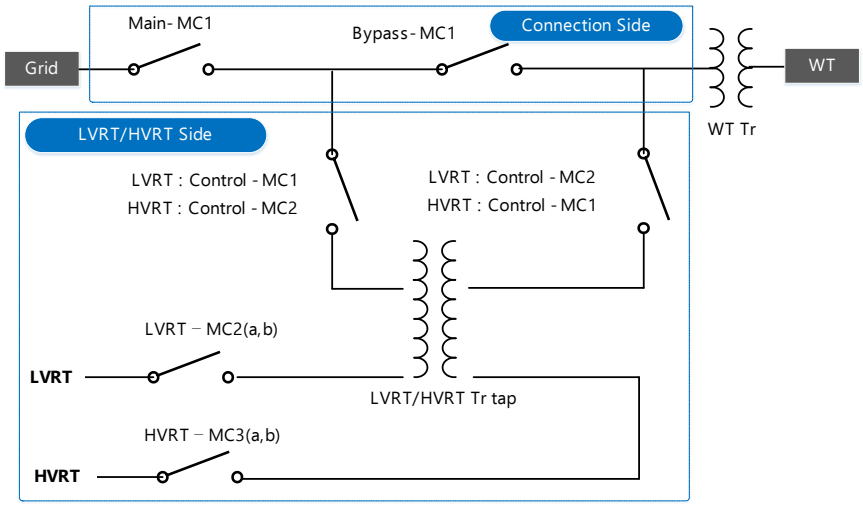

Figure 9. Concept for operation method of LVRT/HVRT test facility.

4.1. Test Facility Operation Strategy in LVRT State

In order to carry out a characteristics test for LVRT, the total windings, including the parallel windings, are connected to the grid side of the test facility, and the parallel windings between the total windings are introduced at the wind turbine side. By considering the proposed connection method, the operation procedure for the LVRT test under the condition that the wind turbine generates normally is composed of a total of three steps, as shown in Figure 10. And the operation strategy for each step can be expressed as follows.

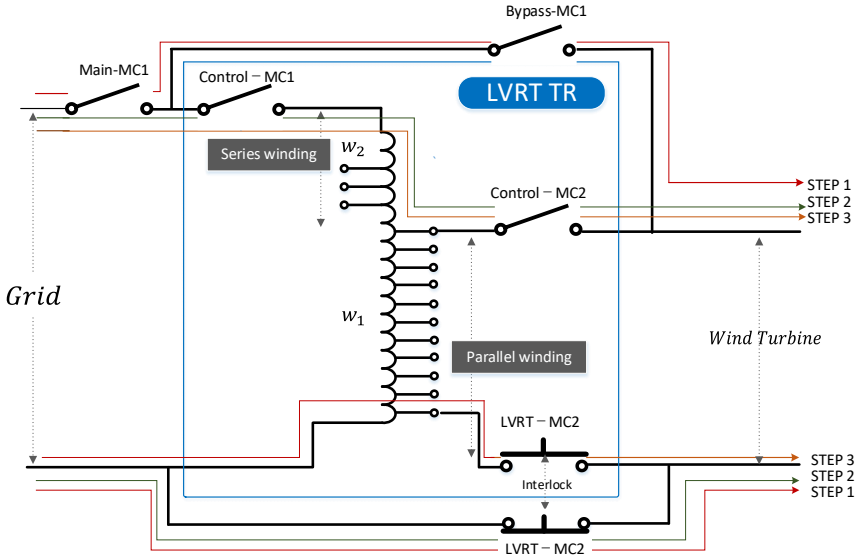

Figure 10. Configuration of the operation method for the LVRT test.

(1) STEP 1: Normal operation
- Standby: power is not applied to the LVRT test facility (the normal state where the voltage sag does not occur due to switches (bypass circuit breaker, selection circuit breaker and control circuit breaker) is the open situation);
- Grid connection: the state in which only the grid and the wind turbine are directly connected without the test facility according to the closed situation of main-MC1 (the main circuit breaker) and bypass-MC1 (the bypass circuit breaker).

(2) STEP 2: Tap operation
- WT-TR connection: the connection state between the shunt tap of the test facility and the wind turbine according to the closed situation of control-MC2 (selection circuit breaker of WT side).
- Parallel operation: the test facility is connected in parallel with the grid according to the closed situation of control-MC1 (the selection circuit breaker of the grid), which is located between the input of series winding in the test facility and grid.
- Series operation: the test facility is connected in series between the grid and WT by bypass-MC1 is open while control-MC2 remains closed (to be kept as a rated voltage).

(3) STEP 3: LVRT operation

The target voltage sag for LVRT is achieved by closing the operation of LVRT-MC2 (a) to be located on the outgoing side (neutral circuit) of the parallel winding during the set time. By the inter-lock function of LVRT-MC2, LVRT-MC2 (b) has an open characteristic when LVRT-MC2 (a) has been closed. Finally, LVRT operation is performed by instantaneously voltage sag during the set time between 0.1 s and 180 s.

4.2. Test Facility Operation Strategy in HVRT State

To perform the characteristics test of HVRT, the circuit is wired opposite to LVRT. In order words, the windings, including the parallel windings, are connected to the wind turbine side of the test facility and the parallel windings among the total windings are introduced at the grid side. As mentioned earlier, the operation procedure of the HVRT test occurs under the condition that the normal wind turbine generation is composed of a total of three steps, as shown in Figure 11. The operation strategy for each step can be expressed as follows.

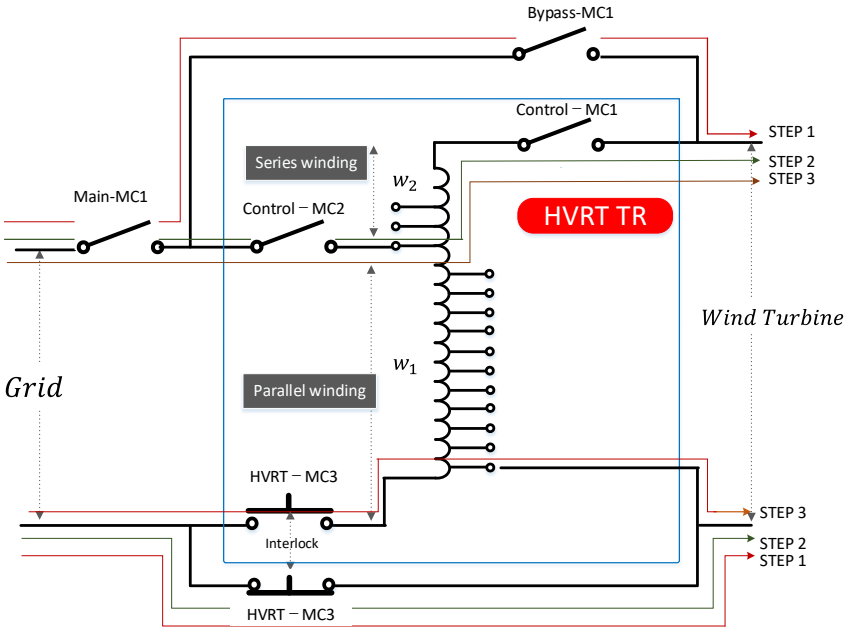

Figure 11. Configuration of the operation method for the HVRT test.

(1) STEP 1: Normal operation

Step 1, including the standby and grid connection, is the same as in the LVRT procedure.

(2) STEP 2: Tap operation

- WT-TR connection: the connection state between the shunt taps of the test facility and the wind turbine according to the closed situation of control-MC1 (selection circuit breaker of the WT side).
- Parallel operation: the test facility is connected in parallel with the grid according to the closed situation of control-MC2 (selection circuit breaker of the grid), which is located between the input of the series winding in the test facility and grid.
- Series operation: the test facility is connected in series between the grid and WT by bypass-MC1 is open while control-MC1 remains closed situation (to be kept as rated voltage.

(3) STEP 3: HVRT operation

The target voltage for HVRT is occurred by closing operation of LVRT-MC3 (a) to be located on the outgoing side (neutral circuit) of parallel winding during the set time. Where, by the inter-lock function of HVRT-MC3, HVRT-MC3 (b) has an open characteristic when HVRT-MC3 (a) has been closed. Finally, HVRT operation is performed by instantaneously voltage sag during the set time between 0.1 s and 600 s.

Therefore, in order to operate the LVRT and HVRT proposed above, the operation procedure of the test considering the operation time is shown in Figure 12.

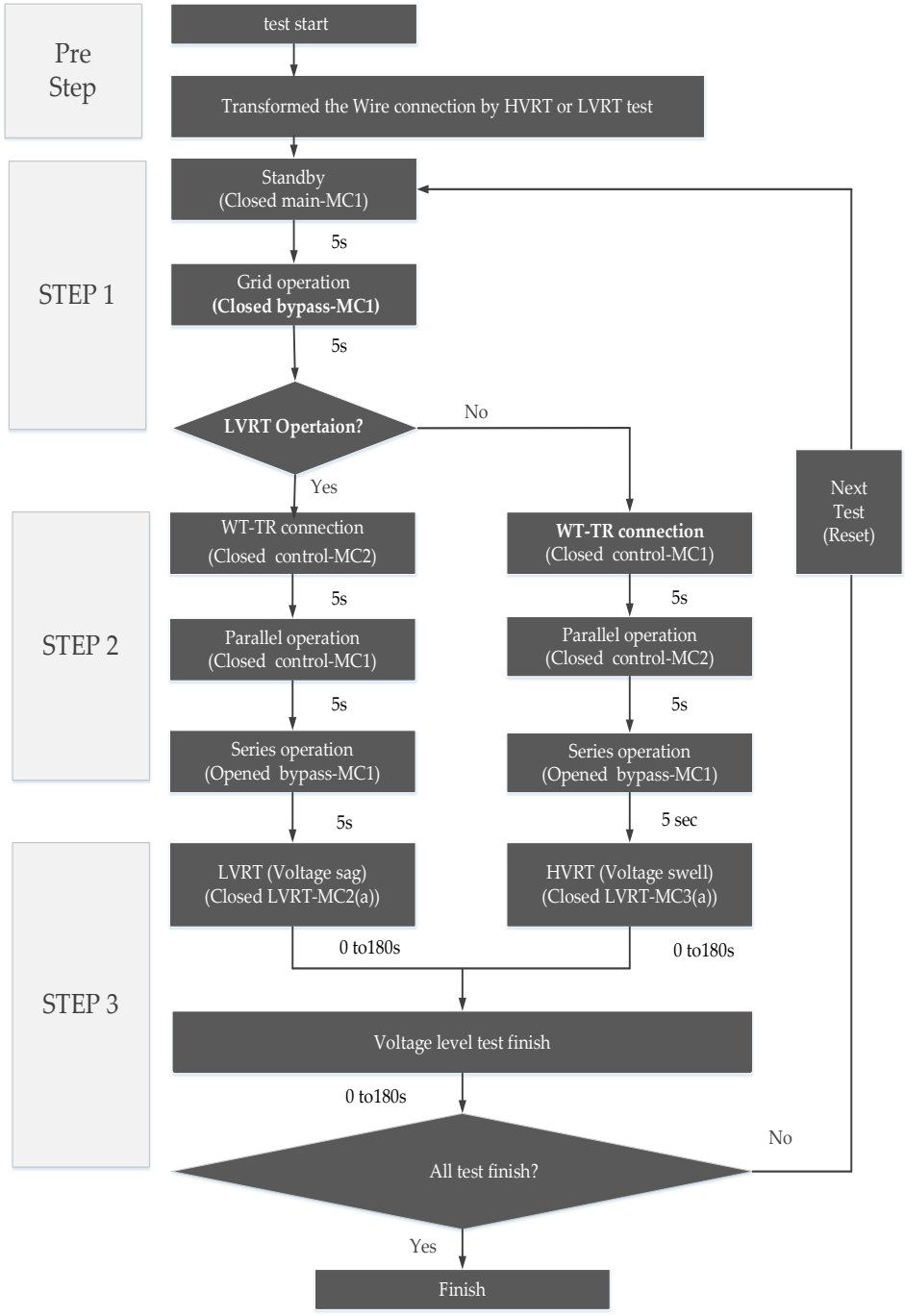

Figure 12. Test procedure considering operation time.

5. Implementation of a 30 kW-Scale Hardware-in-Loop Test System for LVRT/HVRT Performance Evaluation of WT

5.1. Evaluation System for a 30 kW-Scale Hardware-in-Loop Test System

This paper has implemented a 30 kW-scale hardware-in-loop test system composed of a 30 kW-scale LVRT/HVRT facility, power hardware-in-loop system (power HIL-system) and WT hardware-in-loop system (WT HIL system) adapting the data from a 5 MW-scale baseline wind power system, which is provided for the purpose of public research in the national renewable energy laboratory (NREL) [20], as shown in Figures 13 and 14. The WT HIL system is composed of a 1:1 transformer installed at the point of common coupling, a power converter that can demonstrate P-Q output characteristics according to

the characteristics of the wind power generator, and a unidirectional power supply that simulates the power source (a wind power generator).

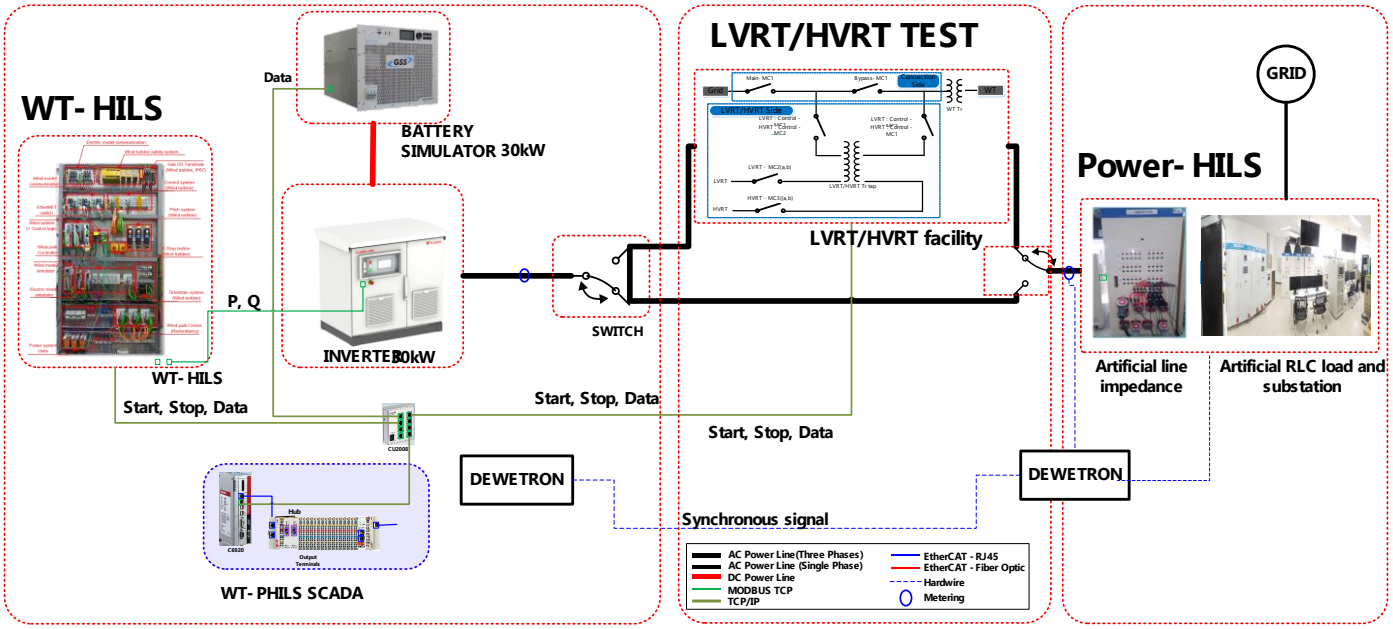

Figure 13. Configuration of a 30 kW-scale hardware-in-loop system.

Figure 14. Implementation of a 30 kW-scale hardware-in-loop system for the evaluation of WT.

5.2. Wind Turbine Hardware-in-Loop System

As a real-time processing-based WT HIL system that is capable of evaluating the performance of the entire control system for wind power generators, the HIL system is composed of a 30 kW-scale power conversion device and control system of the wind turbine, as shown in Figure 15. The control system consists of a mathematical model, signal processing technology and a commercialized control algorithm for the wind turbine. In this paper, the WT HIL system is simulated as a 30 kW scale based on the output characteristics of the actual wind power generator (baseline wind power system model provided for the purpose of public research in NREL) [20].

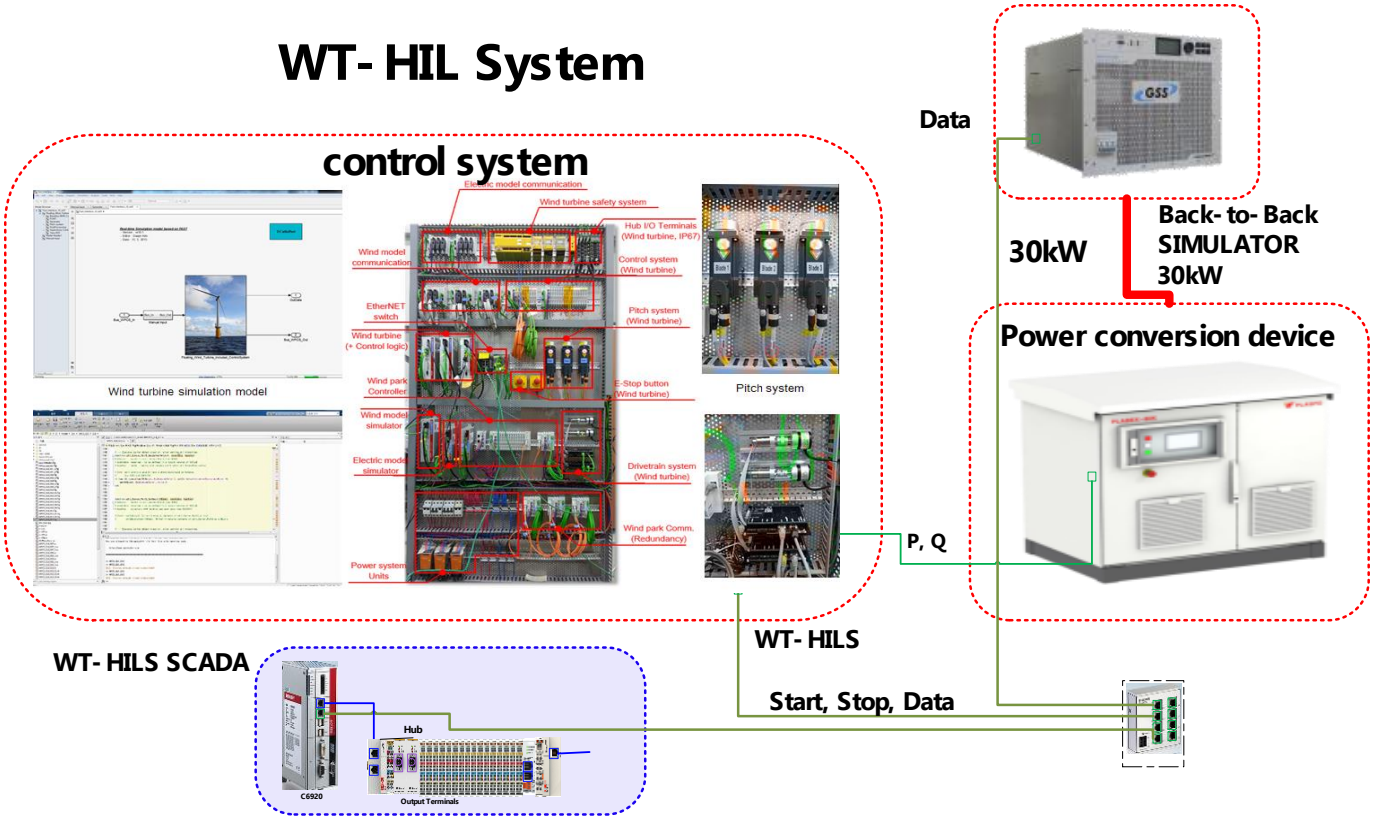

Figure 15. WT hardware-in-loop system.

Table 4 shows the specification of the NREL 5 MW baseline wind turbine, including mechanical properties [20].

Table 4. Specification of NREL 5 MW baseline wind turbine.

Category	Value	Unit
Rated Power	5	MW
Rotor Orientation	Upwind	-
Number of Blades	3	-
Rotor Diameter	126	m
Hub Height	90	m
Cut-In, Rated Rotor Speed	6.9, 12.1	rpm
Cut-In, Rated, Cut-Out Wind Speed	3, 11.4, 25	m/s
Gearbox Ratio	97:1	-
Generator Inertia	534,116	kg m^2
Nacelle Mass	240,000	kg
Tower Mass	347,460	kg

5.3. A 30 kW-Scale LVRT/HVRT Facility

In order to verify the usefulness of the testbed using the tap-change method for site evaluation of LVRT/HVRT in bulk wind power generator, this paper implemented a 30 kW-scale LVRT/HVRT facility, as shown in Figure 16, based on the above-mentioned modeling and operation strategy. This facility adopted multi-stage taps so that they could be divided into series and parallel windings through an intermediate tap using an autotransformer.

Figure 16. A 30 kW-scale LVRT/HVRT facility.

The autotransformer has the advantages of relatively small copper loss and leakage flux because it shares the half-secondary winding in spite of having the same electrical characteristics as the two-winding transformer. Therefore, this paper implemented autotransformer-based equipment using the tap-change method, instead of using the existing RLC method, based on such advantages, and the configuration specification of this equipment is shown in Table 5.

Table 5. Fundamental configuration specification of the facility.

Classification	Detailed Configuration
type of transformer	Air-core & iron-core reactors
rated specification	Phase 60 Hz,
capacity of transformer	30 kVA
Coil	AI 2NC 2.8 × 10.5 × 1H2W
current density	0.79 A/mm^2
No. of turns	72 T (12 T× 6th floor = 72 T)
cooling duct	10 T × 5 = 50 m

5.4. Power Hardware-in-Loop System

In order to analyze the operating characteristics of the distribution system interconnected with a renewable energy source, an HIL power system was implemented by proportionally reducing the 10 MW-scale distribution system to 30 kW, as shown in Figure 17. Specifically, In order words, it system is composed of an artificial distribution line (a total of three sections), artificial customer load and artificial sub-station. Specifically, an artificial distribution line was implemented with adjusting R + jX as a multi-tap method for stimulating a maximum of 40 km of line length. It was designed as a substation with three voltage regulators and a 1:1 transformer, and the customer load in each section (a total of three sections) was simulated using the RLC load.

Figure 17. A 30 kW-scale hardware-in-loop system.

6. Test Results and Analysis

6.1. Test Conditions

In order to verify the feasibility of the operation and design model of the proposed LVRT/HVRT test facility based on the autotransformer, this paper adapts the 10 kW-scale hardware-in-loop wind power system by interconnecting with a 30 kW-scale LVRT/HVRT testbed, as shown in Figure 18, and HIL-Simulator, a wind power simulator by considering the data from 5 MW-scale of a baseline wind power system, which is provided for the purpose of public research in NREL.

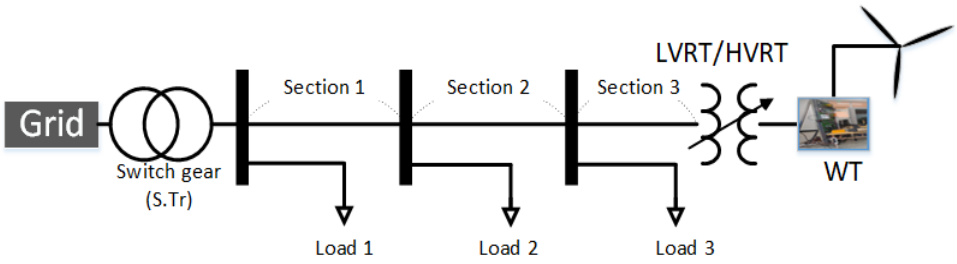

Figure 18. Artificial test grid configuration for LVRT/HVRT test.

On the other hand, the test feeder is considered by a 30 kW-scale power HIL-system (380 V-y) for grid evaluation which is proportionally simulated in 1/100 of the distribution system (22.9 kV-y). The feeder, assuming a total of 2 km, is divided into three sections, with the LVRT facility and WT HIL system at the outgoing location of the end section (third). The reference capacity of the percentage unit is assumed as 1 MW, so 100 MVA is abbreviated to 1/100, and the service transformer is adapted to a value considering the percentage impedance of the distribution molded transformer for switchgear. As aforementioned, the test conditions are shown in Table 6.

In order to verify the effectiveness of the LVRT/HVRT test facility designed by the autotransformer impedance determination method, this paper performed LVRT/HVRT tests according to the reference guidelines of the IEC-61400-21-1 and transmission and distribution facility operation regulations, as shown in Table 7. For the LVRT test, the voltage dips (sag) were tested to four different levels at 0–0.9 PU, presented in IEC-61400-21-1, and the duration time of LVRT was considered according to the relevant transmission and distribution facility operation regulations (grid code of South Korea). Furthermore, in the case of the HVRT test, two different levels should be tested, one maximum voltage dip (swell) and one event dip (average value: 70%) at 50–80% of the overvoltage range capability. And HVRT duration time at maximum voltage dip and one event dip is adapting as 150 ms and 600 ms by considering IEC-61400-21-1 because the grid code of South Korea

is not defined yet. The capability of the wind turbine to handle LVRT and HVRT tests should be demonstrated for wind turbines operating at full load scale (90 to 100%).

Table 6. Artificial test grid data.

Hosting Capacity	S.Tr Ratio	S.Tr Impedance	Line Impedance	Capacity of WT	Rated Current of WT	Line Length
30 kW	0.38 kV/ 0.38 kV	6%	4%	>10 kW	20 A	2 km
Section	Line length	Impedance (%; 1 MVA)	Load		RES	
1	0.4 km	0.8%	2 kW		0	
2	0.8 km	1.6%	2 kW		0	
3	0.8 km	1.6%	1 kW		WT 10 kW (WT HILS)	

Table 7. LVRT/HVRT test conditions.

Test	Voltage Rate (Percent Unit)	Situation	Phase	WT Operating Power	Duration Time
Test 1	0.0 PU	LVRT	3 Phase	Full load	150 ms
Test 2	0.5 PU	LVRT	3 Phase	Full load	900 ms
Test 3	0.9 PU	LVRT	3 Phase	Full load	1500 ms
Test 4	1.1 PU	HVRT	3 Phase	Full load	600 ms
Test 5	1.3 PU	HVRT	3 Phase	Full load	150 ms

6.2. Impedance Determination for LVRT/HVRT Test

Table 8 and Figure 19 show the test results for impedance (series and parallel) value and operation characteristics of the LVRT/HVRT test facility. Meanwhile, based on the proposed impedance calculation method and differential operation procedure of the LVRT /HVRT test facility, as mentioned earlier, this paper is performed to test verification for impedance determination and operation of the LVRT/HVRT test facility. The maximum impedance ($L_{capa}^{max}[H]$), according to the proposed method, was determined as 3.44 mH.

Table 8. Impedance value by 2the two-step layer impedance determination algorithm.

Z (Ω) Uint	Max. Z (Ω) in Case 3 Phase Fault			
0.129 Ω (0.344 mH)	rate capacity (30 kVA)		5.064 Ω (13.44 mH), 45.58 A	
	capacity considering three-phase fault (90 kVA)		1.296 Ω/(3.44 mH), 136.8 A	
Adapted Z Ω	3.44 mH		%Z (1 MVA base)	846%
Voltage	HVRT/LVRT			
	W1 parallel rate	W2 Series rate	Impedance (Determination)		
			Applied Method	Parallel	Series mH
130%	0.77	0.23	Two-step (HVRT)	2.65 mH	0.79 mH
110%	0.83	1.67	Two-step (HVRT)	2.86 mH	0.58 mH
90%	0.9	0.1	Two-step (LVRT)	3.10 mH	0.34 mH
50%	0.5	0.5	One-step (LVRT)	1.00 mH	1.72 mH
0 %	0	1	One-step (LVRT)	0.01 mH	3.44 mH

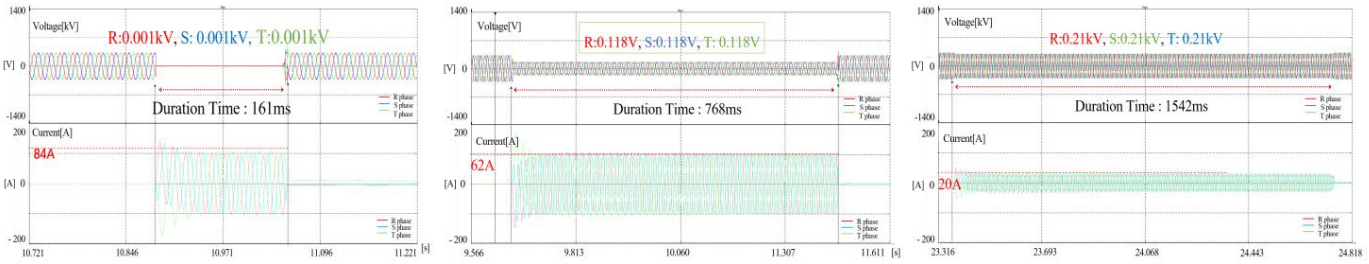

(**a**) (**b**) (**c**)

Figure 19. Results for LVRT test without WT-HILS. (**a**) 0 PU test. (**b**) 0.5 PU test. (**c**) 0 PU test.

Specifically, from Table 7, it was confirmed that the voltage of the auto-transformer was appropriately outputted from 0 to 0.5 PU by the proposed method (impedance determination method). However, the voltages from 0.5 to 1.3 PU not be outputted as accurate values due to a voltage drop caused by series impedance, even though the current, which is determined by parallel impedance, is kept within the allowable range (based on three times the short circuit ratio). Therefore, the parallel and series impedance at voltage levels from 0.7 to 1.3 PU were adapted as re-calculated values by successive approximation methods, as shown in Table 7.

Based on the impedance values mentioned earlier, Figure 19a–c show the voltage characteristics of LVRT when the three-phase voltages were dropped to 0 PU, 0.5 PU, and 0.9 PU for 150 ms, 900 ms, and 1500 ms, respectively. From the test results of LVRT characteristics, as shown in Figure 19 and Table 9, it is clear that the required voltages and operation times in the IEC-61400-21-1 guideline were satisfied in all LVRT tests.

Table 9. Characteristic of test results.

Test No.	Test Condition		Test Results			
	Voltage (Percent Unit)	Duration Time	Voltage (Percent Unit)	Voltage	Duration Time	Current
Test 1	0.0 PU	150 ms	0.01 PU	0.003 kV	161 ms	84 A
Test 2	0.5 PU	900 ms	0.49 PU	0.118 kV	768 ms	62 A
Test 3	0.9 PU	1500 ms	0.94 PU	0.208 kV	1542 ms	20 A

Based on the impedance values mentioned earlier, Figure 20a,b show the voltage characteristics of HVRT when the three-phase voltage is raised to 1.1 PU (operation time: 1350 ms) and 1.3 PU (operation time: 150 ms), respectively. From the test results of the HVRT characteristics, as shown in Figure 20 and Table 10, it is clear that the required voltages and operation times in the IEC-61400-21-1 guideline were satisfied in all HVRT tests.

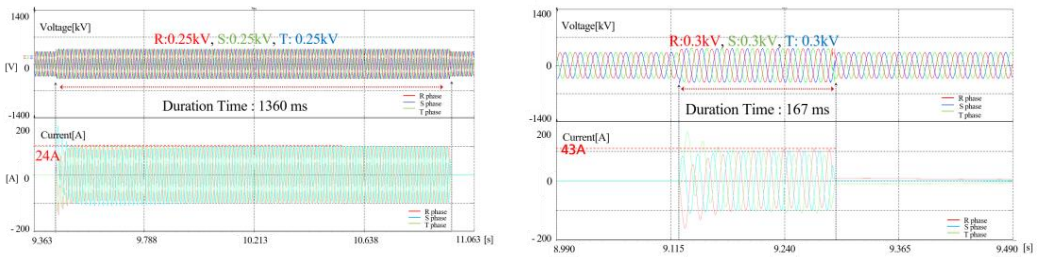

(**a**) (**b**)

Figure 20. Results for the HVRT test without WT-HILS. (**a**) 1.1 PU test. (**b**) 1.3 PU test.

Table 10. Characteristic of test results.

Test	Test Condition		Test Results			
	Voltage (Percent Unit)	Duration Time	Voltage (Percent Unit)	Voltage	Duration Time	Current
Test 4	1.07 PU	1350 ms	1.09 PU	0.24 kV	1360 ms	24 A
Test 5	1.3 PU	150 ms	1.3 PU	0.28 kV	167 ms	43 A

6.3. Impedance Determination for LVRT/HVRT Test

(1) Performance verification

Output characteristic by WT HIL-system is shown in Figure 21 and Table 11. With an output result of 10 kVA, WT hardware-in-loop was simulated based on the output characteristics of the actual wind power generator for 10 min. From the test results for WT output, it is confirmed that the WT HIL system is outputted to reasonable WT characteristics and is a useful tool for performance verification of the LVRT/HVRT test facility.

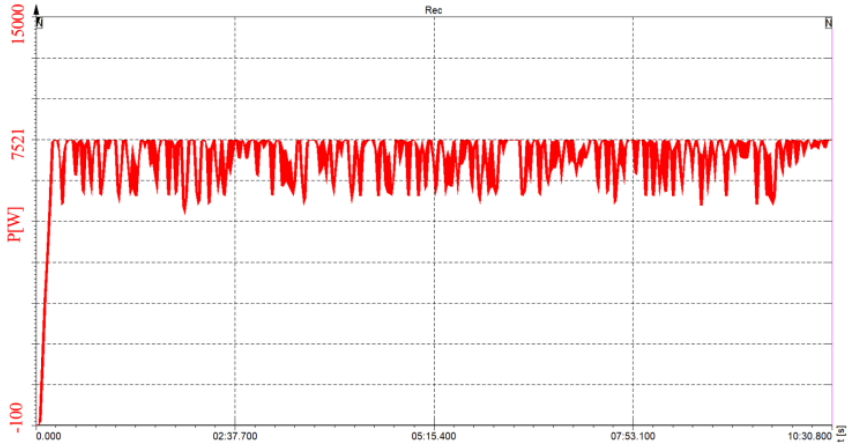

Figure 21. The output performance of WT HILS.

Table 11. WT output for 10 min.

(Average within 10 min) Current	(Average within 10 min) 3 Phase Voltage	(Average within 10 min) Capacity
21 A	378 V	7.57 kW/1.26 kWh

(2) LVRT Test results

- The 0 PU test

Figure 22 and Table 12 show the low voltage characteristics when the-phase voltage is dropped from 1 to 0 PU during the 150 ms by implemented test facility. As a test result of the voltage characteristic at 0 PU (0.001 kV), it is confirmed that the voltage output was maintained at 0 PU as 0.001 kV for 158 ms, and the WT-HILS of 10 kW was not disconnected from the distribution system (380 V-y). Based on the test results, the data summarized during all test periods are expressed in Table 11, where the voltage value means the phase voltage.

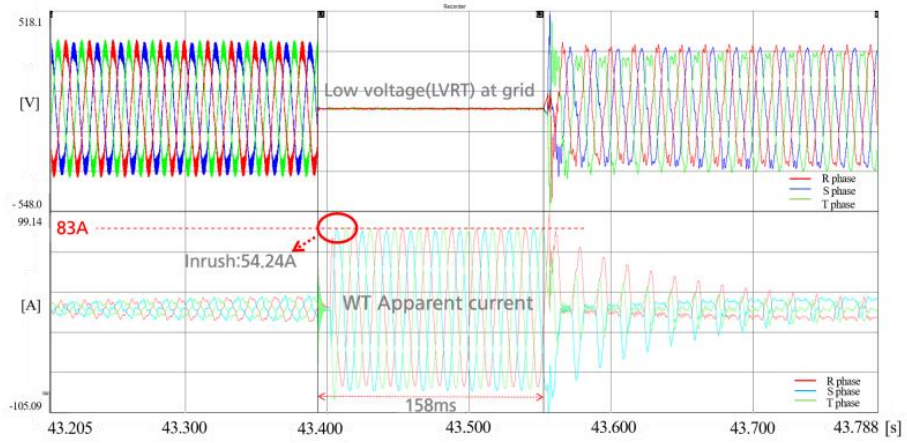

Figure 22. Results of the LVRT test at 0 PU.

Table 12. Analysis of LVRT characteristics at 0 PU.

Before the Test (Steady State)		During the Test (Transient)				After the Test (Steady State)	
WT Output Current		Phase Voltage	WT + Grid Output Current	Test Voltage	Duration Time	WT Output Current	Phase Voltage
Inrush	Steady State						
54 A	20 A	0.219 kV 0.99 PU	83 A	0.00 kV 0.0 PU	158 ms	Within 1 s: 32 A After 1 s: 22 A	0.218 kV 0.99 PU

- The 0.5 PU test

Figure 23 and Table 13 show the result of the low voltage characteristics when the three-phase voltage is dropped from 1 to 0.5 PU (0.11 kV) for 750 ms in the LVRT/HVRT test facility. As a test result of the voltage characteristic, it is confirmed that the voltage output was kept in the 0.5 PU range as 0.115 kV for 768 ms, and the 10 kW WT-HILS was not disconnected from the distribution system (380 V-y). Based on the test results, data summarized during the entire test period are expressed in Table 13.

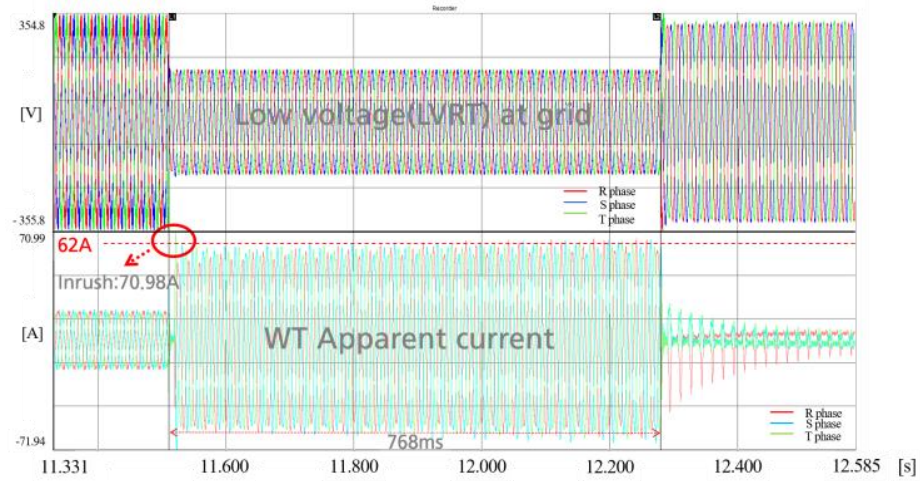

Figure 23. Results of LVRT test at 0.5 PU.

Table 13. Analysis of LVRT characteristic at 0.5 PU.

Before the Test (Steady State)		During the Test (Transient)				After the Test (Steady State)	
WT Output Current		Phase Voltage	WT + Grid Output Current	Test Voltage	Duration Time	WT Output Current	Phase Voltage
Inrush	Steady State						
71 A	20 A	0.219 kV 0.99 PU	62 A	0.115 kV 0.52 PU	768 ms	Within1 s: 33 A After 1s: 16 A	0.216 kV 0.98 PU

- The 0.9 PU test

When the three-phase voltage is controlled from 1 to 1.3 PU by LVRT/HVRT test facility, it is confirmed that voltage output is kept at 0.9 PU as 0.204 kV (0.927 PU) for 0.163 s, as shown in Figure 24. It was also found that the 10 kW WT-HILS was not disconnected from the distribution system (380 V-y) during the test period (0.163 s). Based on the test result, the data summarized during all test periods are expressed in Table 14.

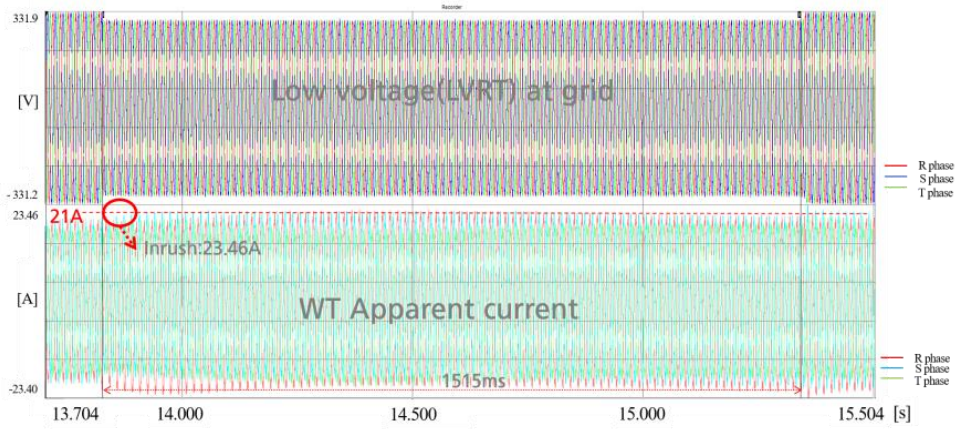

Figure 24. Results of LVRT test at 0.9 PU.

Table 14. Analysis of LVRT characteristic at 0.9 PU.

Before the Test (Steady State)		During the Test (Transient)				After the Test (Steady State)	
WT Output Current		Phase Voltage	WT + Grid Output Current	Test Voltage	Duration Time	WT Output Current	Phase Voltage
Inrush	Steady State						
23 A	21 A	0.219 kV 0.99 PU	21 A	0.204 kV 0.927 pu	1515 ms	Within 1 s: 21 A After 1 s: 21 A	0.219 kV 0.99 PU

(3) HVRT Test Results

- The 1.1 PU test

Figure 25 and Table 15 show the high-voltage characteristics of the LVRT/HVRT test facility when the three-phase voltage was raised from 1 PU (0 V) to 1.1 PU for 1500 ms in the LVRT/HVRT test facility. From the test results of the voltage characteristic at 1.1 PU, it is confirmed that the voltage was kept at 1.1 PU as 0.241 kV (1.09 PU) for 1517 ms, and the 10 kW scale WT-HILS was not disconnected from the distribution system (380 V-y).

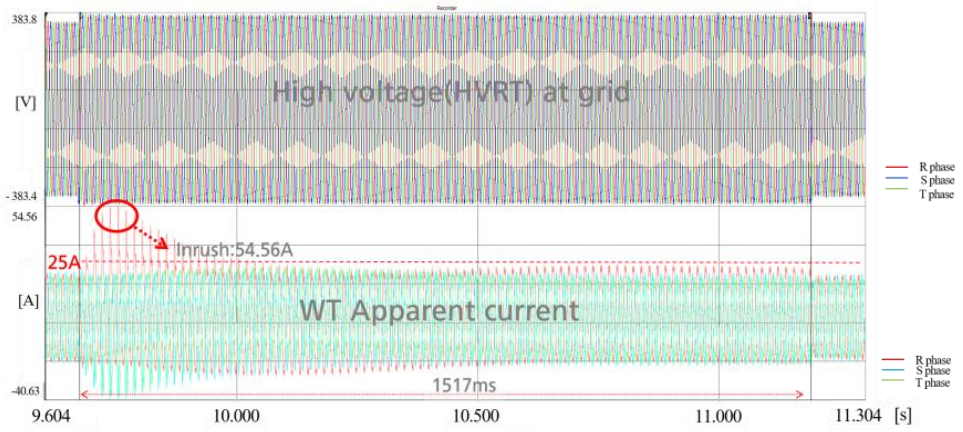

Figure 25. Results of the LVRT test at 1.1 PU.

Table 15. Analysis of HVRT characteristics at 1.1 PU.

Before the Test (Steady State)		During the Test (Transient)				After the Test (Steady State)	
WT Output Current		Phase Voltage	WT + Grid Output Current	Test Voltage	Duration Time	WT Output Current	Phase Voltage
Inrush	Steady State						
54 A	21 A	0.219 V 0.99 PU	25 A	0.241 kV 1.09 PU	1517 ms	Within 1 s: 21 A After 1 s: 21 A	0.219 V 0.99 PU

- The 1.3 PU test

When the three-phase voltage is controlled between 1–1.3 PU in the LVRT/HVRT test facility, it is confirmed that the voltage output was maintained at 1.3 PU as 0.281 kV (1.27 PU) for 168 ms, as shown in Figure 26. It is also confirmed that the 10 kW WT-HILS was not disconnected from the distribution system (380 V-y) during the test period (168 ms). Based on the test result, the data summarized during all test periods are expressed in Table 16, where inrush current only occurred in phase A (82.09 A) due to the short-term operation characteristics.

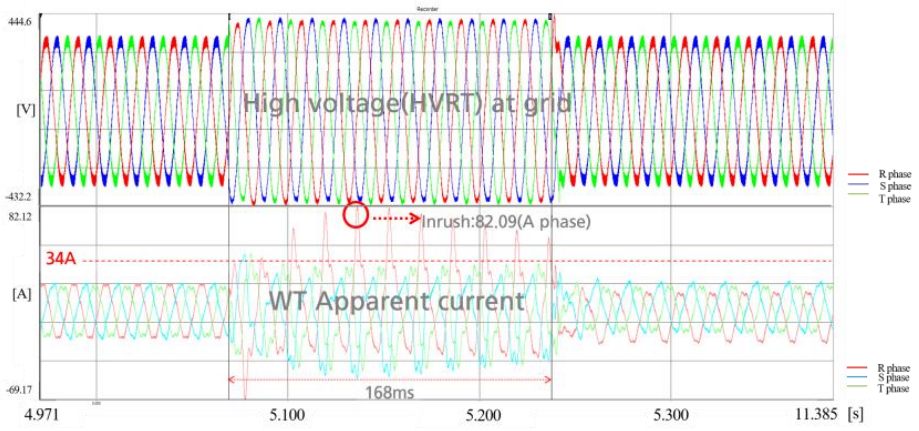

Figure 26. Results of the LVRT test at 1.3 PU.

Table 16. Analysis of HVRT characteristics at 1.3 PU.

Before the Test (Steady State)		During the Test (Transient)				After the Test (Steady State)	
WT Output Current		Phase Voltage	WT + Grid Output Current	Test Voltage	Duration Time	WT Output Current	Phase Voltage
Inrush	Steady State						
82 A	21 A	0.219 V 0.99 PU	34 A	0.281 kV 1.27 PU	168 ms	Within 1 s: 22 A After 1 s: 22 A	0.219 V 0.99 PU

From the voltage characteristic results of all test procedures, it was confirmed that the error range of test voltage was satisfied within 5% of the test guideline of IEC-61400-21-1. It was also found that the duration time of LVRT was exactly maintained as the value time presented by the test guideline of IEC-61400-21-1. Therefore, it is clear that the proposed test strategy and implementation method of the test facility is a useful tool for the dynamic performance verification of WT.

7. Conclusions

This paper proposes an LVRT/HVRT test facility of the autotransformer type, which is capable of outputting the desired voltage range by changing the wiring method and tap position. Furthermore, this paper proposes a detailed calculation method of series/parallel impedance by each voltage level using the proposed fault characteristics-based LVRT/HVRT impedance determination method and successive approximation method. The main results are summarized as follows:

(1) For the operation of the LVRT/HVRT test facility, the wiring method of the autotransformer should be changed according to the overvoltage (HVRT) and undervoltage (LVRT) tests. Under these concepts, this paper proposes a differential operation strategy considering LVRT/HVRT wiring method to perform the stable test when the wind turbine generates power normally;

(2) Using the proposed method, it was confirmed that the voltage of the auto-transformer was appropriately outputted from zero PU to 0.5 PU by the impedance determination method. However, the voltages from 0.5 PU to 1.3 PU were not outputted as accurate values due to a voltage drop caused by series impedance, even though the current determined by parallel impedance was kept within the allowable range (based on three times the short circuit ratio). Therefore, a parallel and series impedance at voltage level from 0.7 PU to 1.3 PU was adapted as re-calculated values by successive approximation method;

(3) From the voltage characteristic results of all test procedures, it was confirmed that the error range of test voltage was satisfied within 5%, presented by the test guideline of IEC-61400-21-1. It was also found that the duration time of LVRT was exactly maintained as the value time presented by the test guideline of IEC-61400-21-1;

(4) Therefore, it is clear that the proposed test strategy and implementation method of the test facility are useful tools for the dynamic performance verification of WT. Furthermore, based on the test results using a 30 kW-scale facility, we plan to apply the operation and tap decision method to a 12 MW facility in future work.

Author Contributions: All of the authors contributed to publishing this paper. B.K. and D.-J.K. carried out modeling and testing and compiled the manuscript. The literature review and data collection were performed by K.-S.R. and Y.-H.N. All authors have read and agreed to the published version of the manuscript.

Funding: This research was funded by the [Ministry of Trade, Industry, and Energy and supported by the Korea Institute of Energy Technology Evaluation and Planning (KETEP)] grant number [No. 20223030020110]. This work was conducted under the framework of the Research and Development Program of the Korea Institute of Energy Research (KIER) (No. C3-2416-01). The APC was funded by [No. 20223030020110].

Data Availability Statement: The data presented in this study are available on request from the corresponding author. The data are not publicly available due to for result test using the equipment owned by our institute.

Conflicts of Interest: The authors declare no conflict of interest.

References

1. Gu, H.; Yan, R.; Saha, T. Review of system strength and inertia requirements for the national electricity market of Australia. *CSEE J. Power Energy Syst.* **2019**, *5*, 295–305.
2. Probert, S.; Nutt, S. *Generator Fault Ride through (FRT) Investigation—Stage 1*; Transpower New Zealand Ltd.: Wellington, New Zealand, 2009.
3. *IEC Standard 61400-21*; IEC 61400: Wind Energy Generation Systems-Part 21-1: Measurement and Assessment of Electrical Characteristics—Wind Turbines 8.5.2.2. IEC: Geneva, Switzerland, 2019.
4. Korea Electricity Security Review, KEEI 2021. Available online: www.iea.org (accessed on 3 May 2023).
5. Karkri, Y.E.; Rey-Boué, A.B.; Moussaoui, H.E.; Stöckl, J.; Strasser, T.I. Improved Control of Grid-connected DFIG-based Wind Turbine using Proportional-Resonant Regulators during Unbalanced Grid. *Energies* **2019**, *12*, 4041. [CrossRef]
6. Arani, M.F.M.; Mohamed, Y.A.R.I. Assessment and Enhancement of a Full-Scale PMSG-Based Wind Power Generator Performance under Faults. *IEEE Trans. Energy Convers.* **2016**, *31*, 735–746. [CrossRef]
7. Kim, K.H.; Jeung, Y.C.; Lee, D.C.; Kim, H.G. LVRT Scheme of PMSG Wind Power Systems Based on Feedback Linearization. *IEEE Trans. Power Electron.* **2012**, *27*, 2376–2384. [CrossRef]
8. Geng, H.; Liu, L.; Li, R.Q. Synchronization and Reactive Current Support of PMSG-Based Wind Farm during Severe Grid Fault. *IEEE Trans. Sustain. Energy* **2018**, *9*, 1596–1604. [CrossRef]
9. Zhong, C.; Wei, L.; Yan, G. Low Voltage Ride-through Scheme of the PMSG Wind Power System Based on Coordinated Instantaneous Active Power Control. *Energies* **2017**, *10*, 995. [CrossRef]
10. Yang, Y.; Blaabjerg, F.; Zou, Z. Benchmarking of Voltage Sag Generators. In Proceedings of the 38th Annual Conference on IEEE Industrial Electronics Society, Montreal, QC, Canada, 25–28 October 2012; pp. 943–948.
11. Park, J.B.; Kim, M.S.; Rho, D.S. Characteristic Analysis and Implementation of 30 kW Portable Test Equipment for Performance Evaluation in Energy Storage System. *Trans. Korean Inst. Electr. Eng.* **2018**, *67*, 715–723.
12. Essl, N.; Renner, H. Influence of LVRT test equipment characteristics on the dynamic performance of a power generation unit quality characteristics of grid connected wind turbines. In Proceedings of the 23rd International Conference on Electricity Distribution, Lyon, France, 15–18 June 2015; p. 1133.
13. Kikusato, H. Performance analysis of grid-forming inverters in existing conformance testing. *Energy Rep.* **2022**, *8*, 73–83. [CrossRef]
14. Saniter, C.; Janning, J. Test bench for grid code simulator for multiMW wind turbines, design and control. *IEEE Trans. Power Electron.* **2008**, *23*, 1707–1715. [CrossRef]
15. Uphues, A.; Nötzold, K.; Wegener, R.; Soter, S.; Griessel, R. Inverter based voltage sag generator with PR-controller. In Proceedings of the 38th Annual Conference on IEEE Industrial Electronics Society, Montreal, QC, Canada, 25–28 October 2012; pp. 1037–1042.
16. Pollanen, R.; Kankainen, L.; Paakkonen, M.; Ollila, J.; Strandberg, S. Full-power converter based test bench for low voltage ride-through testing of wind turbine converters. In Proceedings of the 2011 14th European Conference on Power Electronics and Applications, Birmingham, UK, 30 August–1 September 2011; pp. 1–10.
17. Zeng, R.; Nian, H.; Zou, P. A three-phase programmable voltage sag generator for low voltage ride-through capability test of wind turbines. In Proceedings of the 2010 IEEE Energy Conversion Congress and Exposition, Atlanta, GA, USA, 12–16 September 2010; pp. 305–311.
18. Rainer Klosse. High-Voltage-Ride-Through Test System Based on Transformer Switching. In Proceedings of the 12th International Workshop on Large-Scale Integration of Wind Power into Power Systems as well as Transmission Networks for offshore Wind Power Plant, London, UK, 22–24 October 2013.
19. Wessels, C.; Lohde, R.; Fuchs, F.W. Transformer based voltage sag generator to perform LVRT and HVRT tests in the laboratory. In Proceedings of the 14th International Power Electronics and Motion Control Conference EPE-PEMC 2010, Ohrid, Macedonia, 6–8 September 2010; pp. T11-8–T11-13.
20. Jonkman, J.; Buhl, M.L. *FAST User's Guide*; National Renewable Energy Laboratory: Golden, CO, USA, 2005.

Disclaimer/Publisher's Note: The statements, opinions and data contained in all publications are solely those of the individual author(s) and contributor(s) and not of MDPI and/or the editor(s). MDPI and/or the editor(s) disclaim responsibility for any injury to people or property resulting from any ideas, methods, instructions or products referred to in the content.